J. Phys. G: Nucl. Phys. **9** (1983) 423–441. Printed in Great Britain

The charge and matter distributions of ^{208}Pb

B A Brown†§, S E Massen‡||, J I Escudero‡¶, P E Hodgson‡, G Madurga‡¶ and J Vinas‡*

† Nuclear Physics Laboratory, University of Oxford, Oxford OX1 3RH, UK and Cyclotron Laboratory, Michigan State University, East Lansing, Michigan 48824, USA
‡ Nuclear Physics Laboratory, University of Oxford, Oxford OX1 3RH, UK

Received 4 October 1982, in final form 25 November 1982

Abstract. The best available data on the charge and matter distributions of ^{208}Pb are analysed using (*a*) a Woods–Saxon potential, (*b*) a Hartree–Fock potential based on Skyrme interactions and (*c*) a combination of the two, Woods–Saxon for the surface region and Skyrme–Hartree–Fock for the interior. The single-particle energies and tail densities (or RMS radii) of the valence orbitals are also analysed. The agreement between experiment and theory obtained with potential (*c*) is much better than with (*a*) or (*b*).

1. Introduction

The charge distribution of ^{208}Pb is of particular interest because experimentally it has one of the most accurately measured form factors and because of the doubly magic and spherical nature of this nucleus which makes the theoretical calculations comparatively easy. Moreover there is considerable experimental information from hadron scattering related to the matter (the sum of the point proton and point neutron) densities and from sub-Coulomb one-nucleon transfer reactions related to the properties of the tail densities of the valence orbitals.

We are still a long way from understanding these data starting from first principles, that is from a many-body theory in which the only inputs are the interactions between the nuclear constituents. However, much can be understood qualitatively from phenomenological models which attempt to make predictions for and relationships between observables based on a few underlying parameters. With the models presently available there are several features which have not been well understood. The single-particle potential derived from a realistic finite-ranged nucleon–nucleon interaction should be non-local or, equivalently, energy dependent. The experimental single-particle energy levels, on the other hand, are much closer to what is expected for a simple local potential. Also the charge density is expected to exhibit oscillations due to the shell structure associated with the magic number 82, whereas the experimental charge density shows much less structure.

The goal of this work is limited to the study of what refinements, if any, can be made to

§ Present address: Cyclotron Laboratory, Michigan State University, East Lansing, Michigan 48824, USA.
|| Present address: Department of Theoretical Physics, University of Thessaloniki, Thessaloniki, Greece.
¶ Present address: Departamento Fisica Atomica y Nuclear, Universidad de Sevilla, Sevilla, Spain.
* Present address: Facultad de Ciencias Fisicas, Universidad de Barcelona, Barcelona, Spain.

the existing models to improve the agreement with experiment. This was initiated by the discovery that there already existed in the literature a potential which accounted for both of the above problems, namely the Hartree–Fock potential obtained with the Skyrme VI interaction (Beiner *et al* 1975). The main defect of this potential is that its diffuseness is too small but this can be corrected for most directly by substituting a Woods–Saxon shape for the surface region. At present we cannot provide any good justification for our procedure, but simply provide it as provocative alternative to other approaches. Also we present a much more comprehensive comparison with recent data concerning the single-particle properties than has been provided previously.

The experimental properties of interest are discussed in detail in § 2. In § 3.1 we provide the rationale for our model and a brief historical background of the models leading up to it. The details of the calculation are given in § 3.2 and the choice of parameters is discussed in § 3.3. Comparisons between experiment and theory are made in § 4.

2. Experimental properties

2.1. The experimental charge distribution

From a conceptual point of view it is convenient to have the charge distribution in coordinate space whose Fourier–Bessel transform gives the electron-scattering elastic form factor in the plane-wave Born approximation (PWBA). In fact a great deal of effort has gone into obtaining this charge distribution from a 'model-independent' (MI) distorted-wave Born approximation (DWBA) analysis of the data including relativistic corrections. 'Model independent' means that the shape of the density is abitrary and not dependent on models such as, for example, the Fermi distribution. Some assumptions must be made, however, about the shape of the form factor at high momentum transfer or, equivalently, about how rapidly the density distribution can oscillate. The subtle problems of the MI analysis and the associated historical variations in the results can be traced in the papers by Friar and Negele (1973, 1975), Sprung *et al* (1976), Euteneuer *et al* (1976) and Frois *et al* (1977).

We will use results of an analysis by Sick (1974, 1980) which incorporates the electron scattering data of Frois *et al* (1977), Heisenberg *et al* (1969), Euteneuer *et al* (1976) and Van Niftrik (1969) and the muonic x-ray data of Jenkins *et al* (1971) and Kessler *et al* (1975). A MI charge density has also recently been obtained by Friedrich (1980) using a different method of MI analysis (Euteneuer *et al* 1976). These two charge densities are compared in figure 1 and are seen to be essentially identical except beyond 9 fm (the error band of Sick's density is shown in figures 2–4 and the error band of Friedrich's density is similar).

Our calculations will be concerned only with the proton and neutron degrees of freedom. Thus the total charge distribution should be corrected for the contributions of other virtual particles in the nucleus. To account for the pion-exchange contribution we have subtracted the pion-exchange contribution calculated by Negele and Riska (1978) from the total MI charge distribution. This correction is actually rather small, as can be seen from figure 1. The error band of Sick's experimental charge distribution including the exchange correction is shown and compared with calculations in figures 2–4.

Our calculations initially provide non-relativistic theoretical densities for point protons and neutrons without centre-of-mass corrections. The charge densities are obtained by folding the point densities with the charge densities of the proton (RMS radius $= 0.88$ fm) and neutron (mean-square radius $= -0.116$ fm^2) using the parametrised shape from

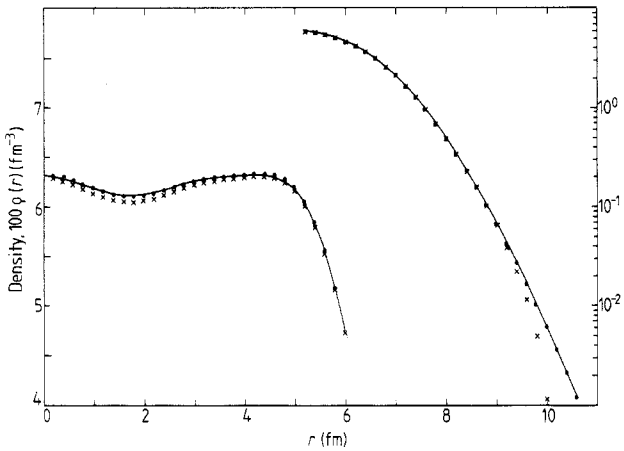

Figure 1. Experimental charge distribution of ^{208}Pb. The results are shown from the analyses of Sick (full curves) and Friedrich (×). Sick's density including the pion-exchange correction is also shown (●); the experimental error band for this density is shown in figures 2–4 with the theoretical calculations.

Chandra and Sauer (1976). In addition corrections are made for the spin–orbit and Darwin–Foldy relativistic effects and for centre-of-mass motion. The details of how these corrections are incorporated are given by B A Brown *et al* (1979).

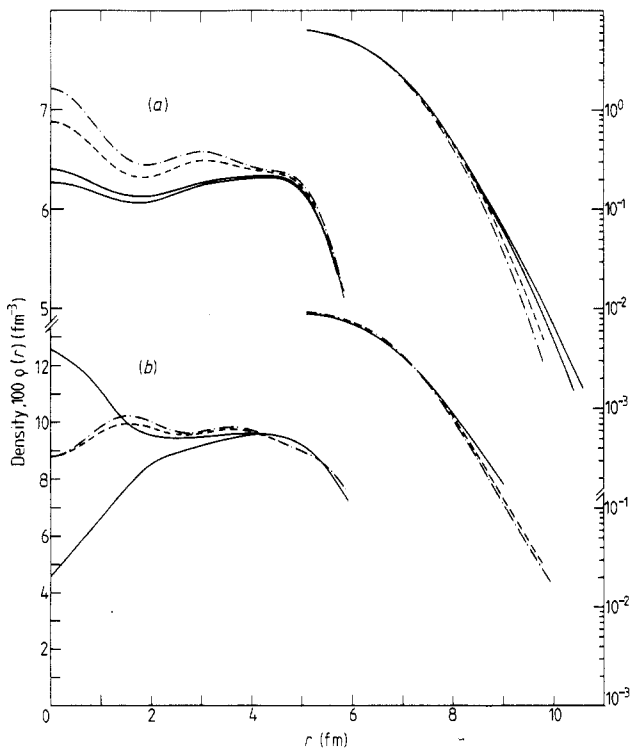

Figure 2. Charge (*a*) and point neutron (*b*) densities: experiment (——) compared with the HF (– · –) and HF + RPA (– – –) calculations of Decharge (1981).

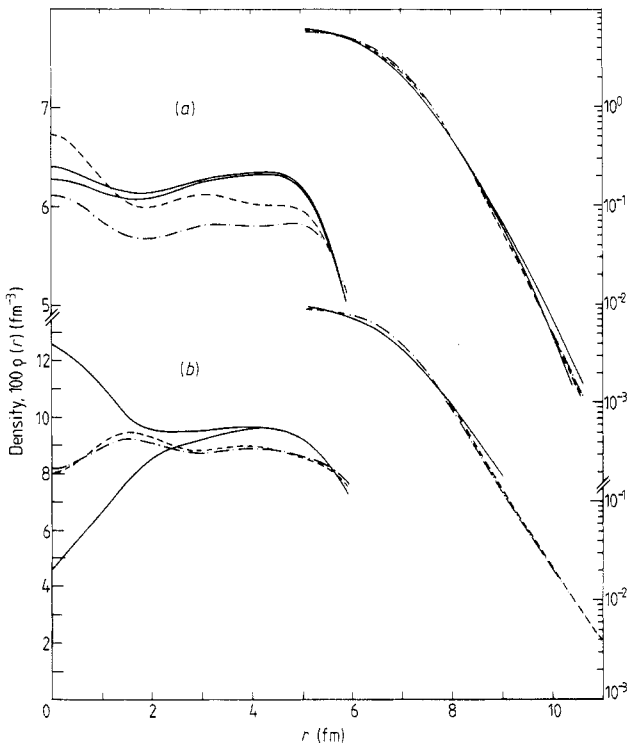

Figure 3. Charge (*a*) and point neutron (*b*) densities. Experiment (——) compared with pure Skyrme calculations: S(0.95) (— · —) and S(0.60) (– – –).

2.2. *Experimental neutron and matter distributions*

Alpha and high-energy (about 800 MeV) proton elastic scattering angular distributions are sensitive to the sum of the neutron and proton densities. We refer to the sum of the point neutron and proton densities as the 'matter' distribution. As in electron scattering, the angular distribution out to the first minimum is primarily sensitive to the RMS matter radius and the further details of the density shape are reflected in the shape of the form factor at higher momentum transfer. Starting from the nucleon–nucleon interactions, a number of experiments have been analysed to provide RMS matter radii and MI density distributions. Since the proton density is known relatively accurately from the charge distribution it is convenient to subtract the proton component to yield the experimental neutron density distribution and the difference in RMS radii $r_n - r_p$. The results of several such analyses are reviewed by Negele *et al* (1979).

We will compare calculations with the MI neutron density determined by Hoffmann *et al* (1980) and shown in figure 2–4. From this analysis, the experimental difference between the proton and neutron RMS radii is $r_n - r_p = 0.14 \pm 0.04$. We note that this neutron density does not take into account the modifications to the Kerman–McManus–Thaler optical potential suggested recently which are required to reproduce the polarised proton scattering data (Hoffmann *et al* 1981).

2.3. *Experimental single-particle energies and spectroscopic factors*

The early (p, d) experiments on ^{208}Pb in which the transfer strengths were observed to be

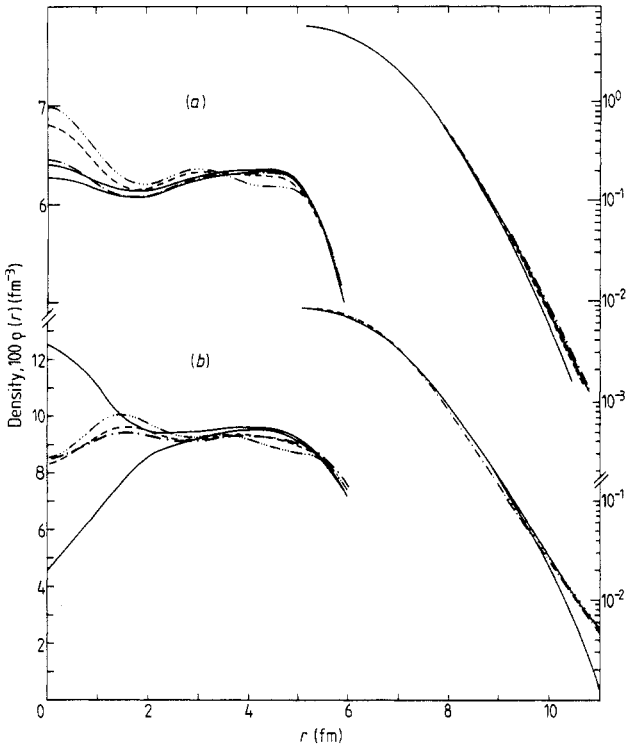

Figure 4. Charge (*a*) and point neutron (*b*) densities. Experiment (——) compared with pure Woods–Saxon calculations ws (— · · · —) and the mixed Woods–Saxon–Skyrme calculations: M(0.95) (— · —) and M(0.60) (– – –).

concentrated in a few low-lying states which nearly exhausted the $(2j + 1)$ spectroscopic sum rules (see Smith *et al* (1971) and references therein) demonstrated the success of the shell model and the closed-shell nature of ^{208}Pb. Most recently the experiments have been extended to high-j inner hole states (Gales *et al* 1979) which are observed to be considerably fragmented.

The states in ^{207}Pb have been studied most extensively and several sets of spectroscopic factors extracted are given in table 1. The results are qualitatively consistent, but beyond the level of about 10%, consistent absolute spectroscopic factors cannot be obtained due to the uncertainties in the optical-model analyses. On the basis of several recent calculations of the non-closed-shell components in ^{208}Pb (Dechargé *et al* 1981, Bernard and Van Giai 1979, 1980, Chu-Hsia and Klemt 1981), reductions of up to about 20% in the spectroscopic strengths are expected. The remaining strength goes into states $2\hbar\omega$ and higher in the particle and hole spectra which are difficult to study experimentally because they are broad with overlapping j values on top of backgrounds from other reaction channels.

For our calculations we assume a closed-shell configuration for ^{208}Pb and thus we will ignore the explicit consequences of this global reduction of the spectroscopic strength and assume that the global reduction is somehow included implicitly in our phenomenological potential. We will, however, consider the local splitting of the strength which has been observed experimentally, most of which is related to multiplets of states arising from the coupling to the low-lying 3^- state in ^{208}Pb. We define the relative spectroscopic factor to

Table 1. Spectroscopic factors for states in ^{207}Pb.

J^π	E_x (MeV)	$C^2S/(2j+1)$ (p, d)[a]	(p, d)[b]	(p, d)[c]	(d, t)[d]	(^{3}He, α)[e]	
$\frac{1}{2}^-$	0.00	0.90	1.08	1.05	1.07	(1.15)	1.00[f]
$\frac{5}{2}^-$	0.57	0.86	1.05	0.98	1.13	1.03	1.00
$\frac{3}{2}^-$	0.90	0.80	0.95	1.00	1.00	(1.75)	1.00
$\frac{13}{2}^+$	1.63	0.67	0.61	0.75	1.04	0.86	0.94
$\frac{7}{2}^-$	2.34	0.55	0.64	1.07	0.89	0.91	0.75
$\frac{9}{2}^-$	3.41	0.49	0.68	0.70	0.98	0.69	0.60

[a] 35 MeV p data from Lanford and Crawley (1974, table III).
[b] 41 MeV p data from Smith *et al* (1971).
[c] Analysis by Satchler (1971) of the 22 MeV p data from Whitten *et al* (1969).
[d] Schmorak (1977).
[e] 70 MeV ^{3}He data of Gales *et al* (1978).
[f] Fraction of total strength observed.

be that for a specific state normalised to the total strength for a specific n, l, j value. The relative spectroscopic factors from the work of Gales *et al* (1978) for ^{207}Pb are given in table 1. These will be used in the interpretation of the neutron tail densities (see § 2.4). Similar information for the particle states is summarised in tables 2 and 3. In addition, the centroid separation energies relative to ^{208}Pb deduced from these experiments will be used to compare with our calculated single-particle energies; for the neutron states these are given in table 4. Experimental information about the proton states has been taken from the compilations (Schmorak 1977, Martin 1977) and centroid energies deduced are given in table 5.

2.4. Experimental tail densities of the valence orbitals

The problems associated with the optical-model analysis are largely eliminated for sub-Coulomb reactions, and this was first exploited by Körner and Schiffer (1971) to extract the asymptotic tail amplitudes for the neutron hole states of ^{208}Pb. Outside the range of the nuclear potential the fall-off of the wavefunction depends only on the experimental

Table 2. (d, p) Spectroscopic factors and centroid energies for levels in ^{209}Pb from Martin (1977).

J^π	E_x (MeV)	C^2S Absolute	Relative
$\frac{9}{2}^+$	0.00	0.83	1.00
$\frac{11}{2}^+$	0.78	0.86	1.00
$\frac{15}{2}^-$	1.42[a]	0.58	0.81
$\frac{5}{2}^+$	1.57	0.98	1.00
$\frac{1}{2}^+$	2.03	0.98	1.00
$\frac{7}{2}^+$	2.49	1.05	1.00
$\frac{3}{2}^+$	2.54	1.09	1.00

[a] The $\frac{15}{2}^-$ centroid energy is 1.78 MeV.

Table 3. Spectroscopic factors for 'particle states' in ^{207}Pb from (d, t) and (^{3}He, α) reactions (Guillot *et al* 1980).

J^π	E_x (MeV)	C^2S	Reaction
$\frac{5}{2}^+$	2.62	0.014	(d, t)
$\frac{7}{2}^+$	2.66	0.006	(d, t)
$\frac{9}{2}^+$	2.73	0.04	(^{3}He, α)
$\frac{11}{2}^+$	3.22	0.08	(^{3}He, α)
$\frac{1}{2}^+$	3.30	0.055	(d, t)

separation energy and hence the amplitude at any point outside the range of the strong interaction completely determines the entire asymptotic behaviour. This amplitude is equal to $C^2S\rho_{nlj}(r=R)$ where $\rho_{nlj}(r)$ is the value of the single-particle wavefunction squared (our normalisation is $4\pi \int \rho_{nlj}(r)r^2\,dr = 1$). The amplitude of the wavefunction is very sensitive to the potential and hence one cannot readily deduce the spectroscopic factor C^2S. Rather, the usual approach is to use the spectroscopic factors measured in the non-sub-Coulomb experiments (§ 2.3) to deduce a value for $\rho_{nlj}(r=R)$ which can be compared with theory.

Historically, the tail densities have been analysed with some assumed form for the single-particle potential in order to deduce the RMS radius of the orbits (Körner and Schiffer 1971, Schiffer and Körner 1973). However, ambiguities in this procedure have been pointed out (Negele 1974) which we prefer to avoid simply by making the comparison between theory and experiment for the tail densities themselves rather than for the RMS radii deduced. We compare with recent data on the proton states (Warwick *et al* 1981, Woods *et al* 1982a, b) (table 6) and the neutron states (Franey *et al* 1979a, b) (table 7).

Table 4. Neutron centroid excitation energies (E_x) and binding energies (BE) for the hole states from Gales *et al* (1978) and for the particle states from tables 2 and 3 combined with ground-state binding energies from Wapstra and Bos (1977).

J^π	(nl)	Centroid E_x (MeV)	Centroid BE (MeV)
$\frac{3}{2}^+$	(3d)		−1.40
$\frac{7}{2}^+$	(2g)		−1.45
$\frac{1}{2}^+$	(4s)		−2.39
$\frac{5}{2}^+$	(3d)		−2.48
$\frac{15}{2}^-$	(1j)		−2.16
$\frac{11}{2}^+$	(1i)		−3.75
$\frac{9}{2}^+$	(2g)		−4.19
$\frac{1}{2}^-$	(3p)	0.00	−7.37
$\frac{5}{2}^-$	(2f)	0.57	−7.94
$\frac{3}{2}^-$	(3p)	0.90	−8.27
$\frac{13}{2}^+$	(1i)	1.87	−9.24
$\frac{7}{2}^-$	(2f)	2.92	−10.29
$\frac{9}{2}^-$	(1h)	4.01	−11.38
$\frac{1}{2}^+$	(3s)	(7.3)	(−14.7)
$\frac{3}{2}^+$	(2d)	(7.6)	(−15.0)
$\frac{11}{2}^-$	(1h)	8.5	−15.9
$\frac{5}{2}^+$	(2d)	(9.0)	(−16.4)
$\frac{7}{2}^+$	(1g)	(10.8)	(−18.2)
$\frac{9}{2}^+$	(1g)	(14)	(−21)

Table 5. Proton centroid excitation energies (E_x) and binding energies (BE) based on (^{3}He, d) and (d, ^{3}He) data from Schmorak (1977) and Martin (1977) combined with ground-state binding energies from Wapstra and Bos (1977).

J^π	(nl)	Centroid E_x (MeV)	Centroid BE (MeV)
$\frac{1}{2}^-$	(3p)	3.97[a]	0.17
$\frac{3}{2}^-$	(3p)	3.12	−0.68
$\frac{5}{2}^-$	(2f)	2.82	−0.98
$\frac{13}{2}^+$	(1i)	1.71[b]	−2.09
$\frac{7}{2}^-$	(2f)	1.50[c]	−2.30
$\frac{9}{2}^-$	(1h)	0.00	−3.80
$\frac{1}{2}^+$	(3s)	0.00	−8.01
$\frac{3}{2}^+$	(2d)	0.35	−8.36
$\frac{11}{2}^-$	(1h)	1.34	−9.35
$\frac{5}{2}^+$	(2d)	1.67	−9.68
$\frac{7}{2}^+$	(1g)	3.48	−11.49

[a] Centroid of the 3.64 and 4.42 MeV $\frac{1}{2}^-$ states in ^{209}Bi.
[b] Centroid of the 1.61 and 2.60 MeV $\frac{13}{2}^+$ states in ^{209}Bi.
[c] Centroid of the 0.90 and 4.45 MeV $\frac{7}{2}^-$ states in ^{209}Bi.

The relative spectroscopic factors discussed in § 2.3 have been divided out to provide an experimental value for $\rho_{nlj}(r)$.

3. Calculations

3.1. Introduction

The initial assumption made in most previous theoretical calculations as well as in those presented here is that the ^{208}Pb ground state has a spherical closed-shell configuration for

Table 6. Point proton single-particle tail densities.

				$\rho(r = 11\text{ fm}) \times 10^7\ (\text{fm}^{-3})$			
					Theory		
J^π	(nl)	Separation energy (MeV)	Assumed strength[a]	Experiment	ws	M(0.95)	M(0.60)
$\frac{3}{2}^-$	(3p)	−0.68	1.0		24.3	28.8	27.9
$\frac{5}{2}^-$	(2f)	−0.98	1.0		11.9	14.3	13.6
$\frac{13}{2}^+$	(1i)	−2.19	1.0		2.0	2.3	2.3
$\frac{7}{2}^-$	(2f)	−2.90	1.0		8.0	9.5	9.2
$\frac{9}{2}^-$	(1h)	−3.80	1.0	1.12 ± 0.11[b]	1.6	1.8	1.8
$\frac{1}{2}^+$	(3s)	−8.01	1.0	3.0 ± 0.7[c]	4.0	4.7	4.4
$\frac{3}{2}^+$	(2d)	−8.36	1.0	1.7 ± 0.4	2.4	2.8	2.7
$\frac{11}{2}^-$	(1h)	−9.35	1.0	0.43 ± 0.11	0.68	0.75	0.75
$\frac{5}{2}^+$	(2d)	−9.68	1.0	1.03 ± 0.24	2.0	2.3	2.2
$\frac{7}{2}^+$	(1g)	−11.49	1.0		0.40	0.43	0.44

[a] C^2S for particle states and $C^2S/(2j+1)$ for hole states.
[b] Warwick *et al* (1981).
[c] Woods *et al* (1982a, b).

Table 7. Point neutron single-particle tail densities.

				$\rho(r=11\text{ fm})\times 10^7$ (fm^{-3})			
					Theory		
J^π	(nl)	Separation energy (MeV)	Assumed strength[a]	Experiment[b]	ws	M(0.95)	M(0.60)
$\frac{3}{2}^+$	(3d)	−1.40	1.0		259	291	307
				337	342	387	409
$\frac{7}{2}^+$	(2g)	−1.45	1.0		83	96	102
$\frac{1}{2}^+$	(4s)	−1.91	1.0	318	335	367	394
$\frac{5}{2}^+$	(3d)	−2.37	1.0		181	203	217
				168	187	210	225
$\frac{15}{2}^-$	(1j)	−2.52	0.81		6.2	6.7	7.7
$\frac{11}{2}^+$	(1i)	−3.16	1.0	6.2	7.4	8.0	9.3
$\frac{9}{2}^+$	(2g)	−3.94	1.0	40	39.3	44.8	49.1
$\frac{1}{2}^-$	(3p)	−7.37	1.0	48	38.7	43.8	47.7
$\frac{5}{2}^-$	(2f)	−7.94	1.0	15.8	15.8	17.7	19.6
$\frac{3}{2}^-$	(3p)	−8.27	1.0	35	30.5	34.4	37.8
$\frac{13}{2}^+$	(1i)	−9.00	0.94	2.2	2.3	2.5	2.9
$\frac{7}{2}^-$	(2f)	−9.71	0.75	10.7	10.7	11.9	13.3
$\frac{9}{2}^-$	(1h)	−10.78	0.60	1.8	1.7	1.7	2.1

[a] C^2S for particle states and $C^2S/(2j+1)$ for hole states (see tables 1 and 2).
[b] The experimental values are from Franey *et al* (1979a, b). (The experimental error is about 10%.)

both neutrons and protons. The Hartree–Fock (HF) theory for a single closed-shell Slater determinant provides the theoretical framework for the relations between the densities and HF potentials and for the relationship $\varepsilon(\text{p/h}) = E(^{208}\text{Pb} \pm \text{one nucleon}) - E(^{208}\text{Pb})$ between the single-particle energies ε and the total binding energies E.

A variety of models and forms have been used previously for the spherical (and generally non-local) single-particle potentials. Some common forms in order of the closeness of their connection with the free-nucleon interaction are as follows.

(1) The Woods–Saxon (Fermi shape) parametrisation.

(2) The HF potential based on the Skyrme interactions.

(3) The HF potential based on approximations to the G matrix plus higher-order corrections.

(4) The HF potential based on the G matrix.

The HF calculations for ^{208}Pb have been reviewed rather thoroughly by Friar and Negele (1975) (see their figure 17 in this paper). We will summarise their conclusions briefly.

Calculations based on the G matrix alone give interior densities which are about a factor of two larger than experiment, indicating a lack of saturation. This situation is improved by about 20% by including the next order in perturbation theory, that is the 2p–2h graphs. Estimates of the higher-order corrections to the binding energies have been made and the resulting improvements suggest that they are needed to further reduce the interior density. Since the exact calculations with these higher-order corrections are technically very difficult to carry out, approximations such as the local density approximation are made in order to simplify the calculation of the G matrix and a phenomenological density-dependent interaction is used to parametrise the effects of higher-order corrections omitted. This leads to the density-dependent HF (DDHF) theories of

Negele (1970) and Dechargé and Gogny (1980) and others discussed by Friar and Negele (1975).

The density-matrix expansion (DME) of Negele and Vautherin (1972) is an approximation to the DDHF theory in which only terms proportional to $\rho(\boldsymbol{r})$ and $\nabla\rho(\boldsymbol{r})$ are kept in an expansion of the nuclear density matrix $\rho(\boldsymbol{r}, \boldsymbol{r}')$. The functional dependence of the potential on the density obtained with the Skyrme interaction (Vautherin and Brink 1972, Dover and Van Giai 1972, Beiner *et al* 1975) has the same general form as that obtained from the DME. This provides a connection with the DME which can be regarded as a justification for using the Skyrme interaction even though it cannot be obtained directly from a short-range expansion of a realistic interaction. Since the DME potential can be expressed analytically in terms of the proton and neutron densities, a physical interpretation of the results can be made more easily and the solution of the Schrödinger equation can be made computationally faster than the full DDHF calculation.

The parameters of the Skyrme interaction have been adjusted to best reproduce the RMS radii and binding energies of spherical nuclei from ^{16}O to ^{208}Pb (Beiner *et al* 1975). However, there remains one unfixed linear combination of parameters which is directly associated with the effective mass (or non-locality). We will consider the Skyrme interaction as a continuous function of the effective mass in nuclear matter m^*/m. This was done by making a quadratic fit for each of the Skyrme parameters to the values given by Beiner *et al* for their interactions VI ($m^*/m = 0.95$), III ($m^*/m = 0.76$) and IV ($m^*/m = 0.47$). Our interaction will be denoted as S(m^*/m) and we will discuss mainly two interactions with rather different effective masses, S(0.60) and S(0.95).

From the DME and Skyrme potentials it is straightforward to understand the physical origins of the density oscillations. Starting with a potential with a flat interior (e.g. a Fermi shape), the oscillations in the proton and neutron densities are nearly exactly out of phase because of the different shell structures associated with the magic numbers 82 and 126. Also, because of the strong attractive proton–neutron interaction, the proton potential is determined primarily from the neutron density and *vice versa*. Hence, for a zero-range two-body interaction, the HF potential is out of phase with the density, which tends to damp the oscillations in a self-consistent calculation. On the other hand, a sufficiently long-ranged interaction can produce a flat potential by washing out the potential oscillations and a further increase in the potential range can produce potential oscillations in phase with the density.

The S(0.60) interaction gives interior potentials and densities which are very similar to those obtained with the DDHF interactions (compare the HF density in figure 2 with the S(0.60) density in figure 3). The S(0.60) HF potential is very flat in the interior and hence the density oscillations are large.

The shape of the interior density obtained with the WS parametrisation is similar to the S(0.60) result in the interior, since both potentials are flat in this region. In the WS parametrisation the radius and diffuseness of the density are controlled by the radius and diffuseness of the potential. Hence, by adjusting the WS potential parameters it is easy to obtain improved agreement for the surface densities compared with those obtained with DDHF and Skyrme interactions. WS calculations with optimised parameters are compared with experiment in figure 4. Attempts have been made to improve the WS calculation by varying the energy dependence of the potential depth and by varying the occupation probabilities, but no significant improvement in the comparison with experiment has been obtained (Hodgson 1979).

The present 'state of the art' for HF calculations based on parametrised nucleon–nucleon interactions is represented by the work of Dechargé and Gogny (1980)

and Dechargé *et al* (1981). Properties of the ^{208}Pb densities they obtain with their interaction 'D1' are shown in figure 2 and in table 8. The biggest improvement in the densities obtained with the D1 interaction over the Skyrme interactions is in the increase of the surface diffuseness. There remain, however, two discrepancies in comparisons with experiment: the theoretical oscillations in the interior charge density are too large and the single-particle energies are too spread out (see figure 10 of Dechargé and Gogny (1980)).

The spreading in the single-particle spectrum has been a long-standing problem (Brown *et al* 1963, Bertsch and Kuo 1968) which has recently received renewed attention (G E Brown *et al* 1979, Bernard and Mahaux 1981, Lejeune 1980, Sartor and Mahaux 1980). It is suggested that this can be explained by the coupling of the single-particle state to collective vibrations, which has the effect of 'clothing' the particles and hence increasing the effective mass to the empirical value of near unity. The coupling to collective states is expected to be 'shaken off' at an energy of about $2\hbar\omega$ above the Fermi surface when the effective mass goes back to the nuclear matter value of $m^*/m = 0.6$–0.7 (G E Brown *et al* 1979). Thus the potential depth as a function of binding energy may be rather complicated. Empirically, in ^{208}Pb all of the known single-particle energies are consistent with an energy-independent potential ($m^*/m = 1$), although in lighter nuclei there is evidence that the deep hole states ($\varepsilon > 20$ MeV) require a smaller effective mass (Bear and Hodgson 1978, Bauer *et al* 1982).

This coupling to collective states will have two important consequences: the HF potential will be modified and the ground-state wavefunction will contain non-closed-shell components. Recently results from microscopic calculations of these effects have been presented for some properties of ^{208}Pb (Dechargé *et al* 1981, Bernard and Van Giai 1979, 1980, Chu-Hsia and Klemt 1981).

Our approach has been to search for a phenomenological potential which takes into account the problems discussed above. By constructing the potential directly rather than from an interaction we lose the ability to calculate the total binding energy; however, there are many other interesting single-particle properties with which we can compare. Our initial idea was very simple, but turned out to work remarkably well. The potential calculated with the Skyrme interaction was kept for the nuclear 'interior' but the 'surface' was replaced by a Fermi (Woods–Saxon) shape. A method was then found to fix the six

Table 8. Comparison of experimental and theoretical single-particle energies and moments of the densities.

	ε_p $(3s_{1/2})$ (MeV)	ε_n $(3p_{1/2})$ (MeV)	r_{ch} (fm)	$r_n - r_p$ (fm)	$\tilde{a}_{ch}$ (fm)	$\tilde{a}_n$[a] (fm)	r_p[a] (fm)	$\tilde{a}_p$[a] (fm)
Experiment	−8.01	−7.37	5.503[b]	0.14[c]	0.514[b]	(0.547)[d]	5.447	0.465
S(0.95)	−6.89	−6.88	5.587	0.102	0.469	0.506	5.532	0.402
S(0.60)	−7.94	−7.51	5.541	0.158	0.487	0.522	5.485	0.434
HF(D1)[e]	−9.2	−7.9	5.431	0.130	0.490	0.542		
HF(D1) + RPA[f]			5.457	0.126	0.501	0.550		

[a] These are the values for point nucleons including the centre-of-mass correction.
[b] Sick (1974, 1980).
[c] Hoffmann *et al* (1980).
[d] See text.
[e] Dechargé and Gogny (1980) and Dechargé (1981).
[f] Dechargé *et al* (1981) and Dechargé (1981).

potential parameters (the depth, radius and diffuseness for protons and neutrons) unambiguously to six experimental data (see § 3.3).

The major defects in the original calculations with the Skyrme interaction are that the long-range component in the interaction is cut off and the surface nature of the coupling with collective states is not taken into account. These defects will be most important for the surface of the potential and can obviously be corrected by our surface parametrisation. The major defect in the usual Woods–Saxon parametrisation of the entire potential is that the interior is assumed *ab initio* to be flat and our potential corrects for this by allowing a connection with the underlying nucleon densities via the Skyrme interaction.

We have not considered the contributions from the non-closed-shell components in the ^{208}Pb ground state and will assume that this effect is relatively small. Recently the non-closed-shell contributions to the densities have been calculated in the framework of a HF plus random-phase approximation (RPA) model (Dechargé *et al* 1981). In figure 2 we show the charge and neutron densities calculated by Dechargé (1981). The difference between the HF and HF + RPA densities may be understood as a combination of effects due to a change in the potential and due to a change in the orbit occupations. To the extent to which the latter effect can be separated from the first, which is unknown to us at present, the effects due to the change in the orbit occupations should be considered as a correction to our calculations.

3.2. Details of the calculations

The Skyrme two-body interaction leads to a non-local HF potential with eigenfunctions $\psi(r)$ and eigenvalues ε which can be obtained using a local but energy-dependent potential in the equation (Dover and Van Giai 1972):

$$\left(-\frac{\hbar^2}{2\mu}\frac{\mathrm{d}^2}{\mathrm{d}r^2}+\frac{\hbar^2}{2\mu}\frac{l(l+1)}{r^2}+U_{\mathrm{L}}(r,\varepsilon)\right)\psi_{\mathrm{L}}(r)=\varepsilon\psi_{\mathrm{L}}(r) \tag{1}$$

where

$$\psi(r)=(m^*(r)/m)^{1/2}\psi_{\mathrm{L}}(r) \tag{2}$$

$$U_{\mathrm{L}}(r,\varepsilon)=(1-m^*(r)/m)\varepsilon+(m^*(r)/m)U(r) \tag{3}$$

and

$$m^*(r)/m=[1+C_0(\rho_{\mathrm{p}}(r)+\rho_{\mathrm{n}}(r))\pm C_1(\rho_{\mathrm{p}}(r)-\rho_{\mathrm{n}}(r))]^{-1} \tag{4}$$

In the last equation the plus sign refers to protons and the minus sign to neutrons. For historical reasons, we use the usual reduced mass, $\mu=m_\tau(A-1)/A$ (τ=p or n), for the Woods–Saxon calculations and a reduced mass for the Hartree–Fock calculations which includes a centre-of-mass correction for the total energy (Vautherin and Brink 1972), $\mu=m_\tau A/(A-1)$.

The potential $U(r)$ is divided in the usual way into a central, spin–orbit and Coulomb interaction:

$$U(r)=V(r)+V_{\mathrm{so}}(r)\langle \boldsymbol{l}\cdot\boldsymbol{\sigma}\rangle+V_{\mathrm{Coulomb}}(r)\delta_{\mathrm{pn}} \tag{5}$$

where δ_{pn} is equal to 1 for protons and 0 for neutrons.

We will consider three approximations for the central potential $V(r)$: the Woods–Saxon

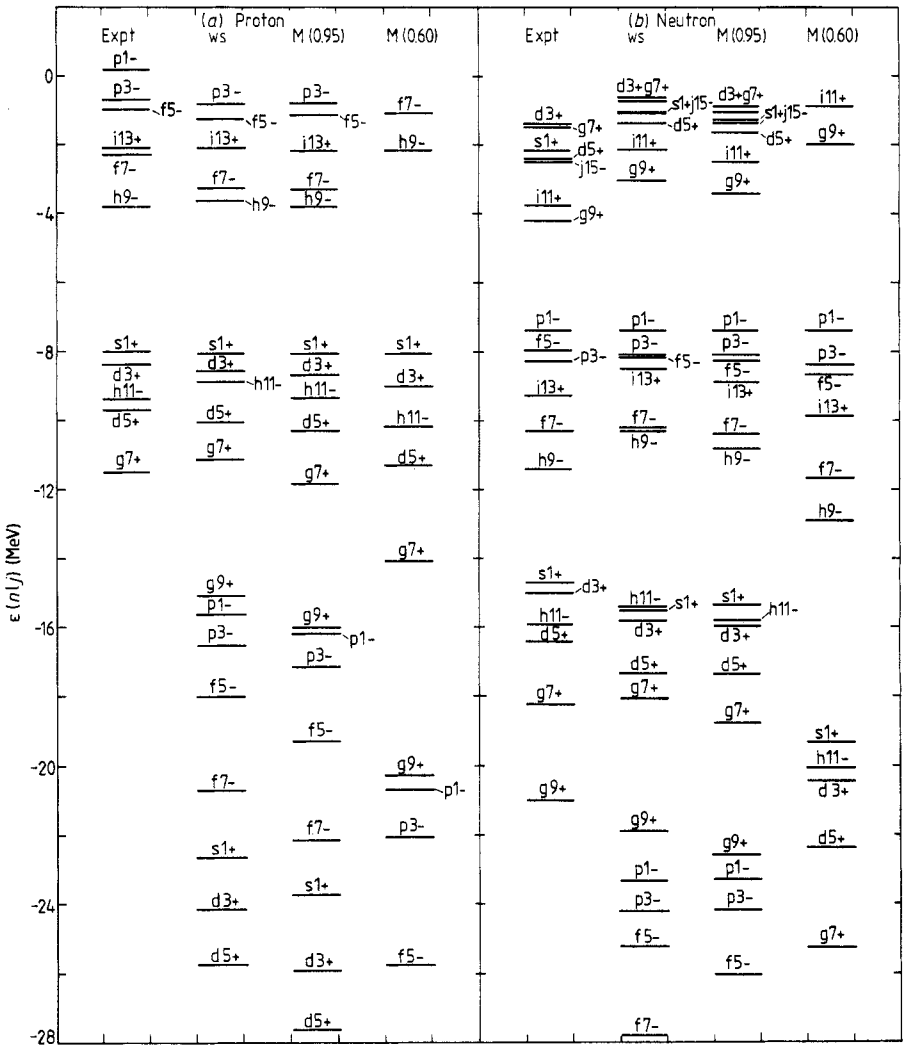

Figure 5. Experimental centroid energies of the proton (*a*) and neutron (*b*) single-particle states compared with the ws, M(0.95) and M(0.60) calculations. The states are labelled by l, $2j$ and parity.

potential $V_W(r)$, the Skyrme potential $V_S(r)$ and a mixture of these two, $V_m(r)$:

$$V_W(r) = V_\tau\{1 + \exp[(r - R_\tau)/a_\tau]\}^{-1} \tag{6}$$

$$V_S(r) = F(\rho_p(r), \rho_n(r)) \tag{7}$$

$$\begin{aligned} V_m(r) &= V_W(r) \qquad \text{for } r \geqslant 5 \text{ fm} \\ &= V_S(r) \qquad \text{for } r < 5 \text{ fm}. \end{aligned} \tag{8}$$

V_τ, R_τ and a_τ are the constants for the well depth, radius and diffuseness for the proton and neutron Woods–Saxon potentials. The Skyrme functional F of the proton and neutron densities is given by Dover and Van Giai (1972); this is the quantity inside the first square

bracket in their equation (2.12) (note that in their equation (2.5) the term $\frac{1}{2}(t_1 + t_2)$ should be replaced by $\frac{1}{4}(t_1 + t_2)$).

For the mixed potential the radius of 5 fm is chosen because it corresponds to the top of the potential shoulder for ^{208}Pb (see figure 6). We have not explored the sensitivity to different choices of this matching radius. To remove a possible kink, the mixed potential was smoothed over an interval of about 0.5 fm around the matching radius. In the mixed potential calculations the effective mass of equation (4) was used for all radii.

The purely Woods–Saxon calculations we present were obtained with an effective mass of unity. The interior of the calculated densities is changed very little if a smaller effective mass (or the almost equivalent Perey–Buck (1962) correction) is used, as long as the ws parameters are readjusted to reproduce the quantities described in § 3.3. For the Skyrme and mixed potentials an effective mass is used with the constants in equation (4) obtained from the Skyrme interaction:

$$C_0 = \frac{2m}{\hbar^2}\left(\frac{5t_2 + 3t_1}{16}\right) \qquad C_1 = \frac{2m}{\hbar^2}\left(\frac{t_2 - t_1}{16}\right). \tag{9}$$

Standard forms are used for the Coulomb and spin–orbit terms in equation (5). For the Skyrme and mixed interaction calculations we use the Coulomb potential calculated by folding the Coulomb interaction with the calculated charge density $\rho_{ch}(r)$ plus an approximation for the exchange term (Beiner *et al* 1975):

$$V^{ex}_{Coulomb}(r) = -\left(\frac{3}{\pi}\rho_{ch}(r)\right)^{1/3} e^2. \tag{10}$$

For the pure Woods–Saxon calculations we use the approximation for the Coulomb potential based on a uniform charge density distribution which has total charge number $Z - 1$ and the experimental RMS charge radius.

For the pure Skyrme calculations we use the Skyrme spin–orbit potential given by Dover and Van Giai (1972) (the first term on the right-hand side of their equation (2.6)) and for the pure Woods–Saxon and mixed potential calculations discussed here we use the usual derivative of the Fermi shape form with strength $(\hbar/m_\pi c)^2 U_{so} = 12$ MeV, radius $1.1A^{1/3}$ fm and diffuseness 0.65 fm. We have also used the Skyrme spin–orbit potential

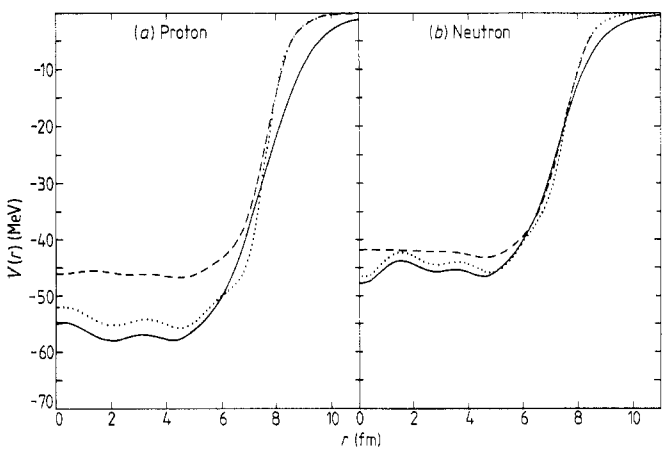

Figure 6. Central potentials for the protons and neutrons. The pure Skyrme potentials S(0.60) (– – –) and S(0.95) (· · ·) and the mixed potential M(0.95) (——).

together with the mixed central potential and have found that the results (except for the details of the n and l dependence of the spin–orbit splitting) are insensitive to this change in the spin–orbit potential. An adjustment of the spin–orbit potential could be considered if we were to include fits to the spin–orbit splittings in our analysis. However, we believe that the present spin-orbit potentials being used are reasonable, and that our conclusions are insensitive to reasonable variations in these spin–orbit potentials.

3.3. Parameters of the potentials

We have chosen the depth, radius and diffuseness parameters of the Woods–Saxon and mixed potentials in order to reproduce exactly some analogous experimental quantities: the single-particle energy of one orbit near the Fermi surface, and the radius and diffuseness of the density. The proton and neutron potentials and properties are considered independently. The parameters were obtained by the usual techniques for non-linear least-squares fitting.

More precisely, we have chosen to reproduce the single-particle energies $e(\text{neutron}, 3p_{1/2}) = -7.37$ MeV and $e(\text{proton}, 3s_{1/2}) = -8.01$ MeV. We characterise the radii and the diffusenesses by the r^2 and r^4 moments of the charge and point neutron density distributions.

It is convenient to combine these second and fourth moments to obtain a measure of the diffuseness. A good approximation for the moments of a Fermi distribution when (a/R) is small is

$$(r_L)^L = \left(\frac{3R^L}{L+3}\right)[1 + \tfrac{1}{6}L(L+5)\pi^2(a/R)^2 + \ldots] \tag{11}$$

where

$$(r_L)^L = \int \rho(r) r^L \, d\tau \Big/ \int \rho(r) \, d\tau. \tag{12}$$

Therefore, based on these equations, we define the quantity $\tilde{a}$ by

$$\tilde{a} \equiv \left(\frac{3(\tilde{r}_4 - \tilde{r}_2)(9\tilde{r}_2 - 7\tilde{r}_4)}{2\pi^2}\right)^{1/2} \tag{13}$$

where

$$\tilde{r}_L = (\tfrac{1}{3}L + 1)^{1/L} r_L. \tag{14}$$

The RMS radius and diffuseness are accurately determined experimentally for the charge distribution (see table 8). We have used the point neutron distribution determined by Hoffmann *et al* (1980) to fix the point neutron RMS radius, but this value is much less certain than the charge RMS radius and we would feel free to change it on the basis of the comparisons with the neutron single-particle energies and tail densities (but in fact we have not had to).

The neutron diffuseness is even less certain. For this reason initially we had arbitrarily decided simply to make the diffuseness of the proton and neutron potentials equal. However, we found that the agreement with the experimental neutron single-particle energies and tail densities could be very much improved by requiring instead that the neutron potential diffuseness give a point neutron density diffuseness of 0.547 fm (the last digit is not significant). This is, in fact, quite close to the value of 0.558 fm obtained from

the neutron density of Hoffmann *et al.* Also we note that the difference between these empirical point proton and neutron diffusenesses is very close to that predicted by the pure Skyrme HF calculations (see table 8).

The potential parameters required to reproduce these properties are given in table 9.

4. Comparison with experiment

The charge and point neutron densities obtained with the mixed potentials based on two values of the Skyrme effective mass, M(0.60) and M(0.95), are compared with experiment in figure 4. The general agreement for the charge density is, of course, not surprising since the potential parameters were chosen to exactly reproduce the r^2 and r^4 moments. However, the detailed agreement obtained with the M(0.95) potential is remarkable. We note that the general M(m^*/m) results would be represented by a continuous family of curves between the M(0.60) and M(0.95) results shown, and from this it can be seen that the optimal agreement with experiment is, in fact, obtained with $m^*/m = 0.95$ (although this was not a fitted parameter).

The tail of the experimental charge density is well reproduced with both the M(0.60) and M(0.95) potentials. This is partly due to the trivial fact that the two moments r^2 and r^4 are fitted. The roughly exponential fall-off of the tail densities is determined by the contribution from the many individual valence orbits which in turn is determined by their separation energies. The separation energies are shown in figure 5. Since the separation energies of the filled orbitals are larger with the M(0.60) potential than with the M(0.95) potential one would expect the calculated tail densities to fall off faster. In our calculations this effect is mostly compensated for by the readjustment of the shape of the potentials in each case to give the same r^2 and r^4 moments of the total density. The general overbinding of the single-particle energies in the HF(D1) calculation (see figure 10 of Dechargé and Gogny (1980)) shows up in the too rapid fall-off in the tail of the theoretical charge density compared with experiment as seen in figure 2. We note that the faster fall-off in the charge density immediately beyond 9 fm obtained in the model-independent analysis of Friedrich (1980) is not realistic compared with theoretical expectations.

The experimental and calculated tail densities for the proton and neutron orbits are compared in tables 6 and 7, respectively. Since the calculated tail amplitudes are sensitive in a trivial way to small differences in the separation energies, the theoretical values were not based on the theoretical single-particle energies shown in figure 5 but on the experimental separation energies for each state as given in tables 6 and 7 which were reproduced by renormalising the central potential by a multiplicative constant independently for each state.

The experimental proton tail densities are consistently smaller than our calculations (see table 6) which is surprising given the good agreement we have obtained for the charge

Table 9. Potential parameters.

Potential	$V_p(r=5$ fm) (MeV)	$V_n(r=5$ fm) (MeV)	$R_p/A^{1/3}$ (fm)	$R_n/A^{1/3}$ (fm)	a_p (fm)	a_n (fm)
ws	58.050	44.902	1.2675	1.2284	0.8115	0.6604
M(0.95)	56.003	45.652	1.2694	1.2183	0.8749	0.7295
M(0.60)	46.384	43.145	1.2865	1.2179	0.7620	0.6612

density and proton single-particle energies. A possible explanation is that the spectroscopic factors are actually smaller than our assumed values of 1.0 due to fragmentation with other states. However, as noted by Chapman (1982), the major contributions to the errors in the results from the $^{208}Pb(t, \alpha)^{207}Tl$ experiment of Woods *et al* (1982a, b) are from the uncertainties in the (t, α) normalisation factor and the uncertainties in the optical-model parametrisation of the distortion effects. The relative magnitudes of the experimental proton tail densities, which are less sensitive to these systematic uncertainties, are in better agreement with theory. It would be worthwhile to repeat these experiments with sub-Coulomb heavy-ion reactions.

The point neutron distribution of Hoffmann *et al* (1980) shown in figure 4 is not as well reproduced by any of the calculations as was the charge distribution, even though all of the curves shown in figure 4 have nearly the same r^2 and r^4 moments (see § 3.3 and table 8). It seems that the general shape of the experimental curve beyond 5 fm is inconsistent with the theoretical shape. The error band on the 'experimental' neutron density includes only the true experimental uncertainties and not those due to systematic errors in the optical-model analysis. Recent analyses of polarised proton scattering data indicate that refinements are needed in the usual Kerman–McManus–Thaler optical-model potentials (Hoffmann *et al* 1981).

As mentioned in § 3.3, other information about the neutron states indicates that the moments of the neutron density that we have chosen are reasonable. Most importantly, the tail densities of the valence neutron orbits are in agreement with experiment within the assumed experimental uncertainty of 10% (see table 7). By refitting the potential to give a point neutron RMS radius 1% larger but not allowing the diffuseness to change (corresponding to an increase in $r_n - r_p$ from 0.14 fm to 0.19 fm), the amplitudes of the tail densities are increased on average by 10%. And by refitting the potential to give a point neutron diffuseness 5% larger but not allowing the RMS radius to change, the tail densities are increased on average by 15%. Also, the single-particle energies depended on the moments of the density fitted. The potential fitted to give a point neutron diffuseness 5% larger, but not allowing the RMS radius to change, raised the centroid of the $1i_{13/2}-1i_{11/2}$ spin–orbit pair relative to the $3p_{3/2}-3p_{1/2}$ spin–orbit pair by 0.85 MeV. In all cases these changes make the agreement with experiment worse.

Finally, in order to show clearly the differences between our mixed potentials and the unmodified Skyrme potentials, the central potentials for protons and neutrons are plotted in figure 6. The oscillatory nature of the interior of the S(0.95) and M(0.95) potentials relative to the flat S(0.60) potential is clearly shown.

5. Summary

Starting with a closed-shell configuration for ^{208}Pb, a phenomenological potential can easily be found which essentially reproduces single-particle density properties within experimental errors and the single-particle energies within a few hundred keV. This was obtained by combining the Hartree–Fock potential obtained with Skyrme interactions for the interior with a phenomenological Fermi shape for the surface.

The interior oscillations of the proton and neutron densities are sensitive to the oscillations of the potential. The relatively flat potentials which are obtained with the Skyrme ($m^*/m = 0.60$) HF and with Negele's DDHF calculations do not reproduce the experimental charge density. The oscillations present in the Skyrme ($m^*/m = 0.95$) potential are required to obtain better agreement. Given that this interaction also gives the

best agreement for energy levels, this result is not unexpected. However the connections on a deeper level remain to be understood.

The shape of the interior density is dependent upon which orbitals are being filled and their occupation probabilities as well as upon the shape of the potential. Occupation probabilities deduced empirically from the observed oscillations will therefore depend strongly on what is assumed about the potential and *vice versa*. The initial calculations which include explicitly the effects of the non-closed components on the densities (Dechargé *et al* 1981) are encouraging but further work needs to be done to improve the agreement with experiment.

Our mixed potential model can easily be extended to other nuclei, as long as the six parameters of the surface Fermi shape are readjusted for each nucleus. It is well known that on average the potential radius goes as $A^{1/3}$ and that the diffuseness and well depth are constant. This prescription provides a method for a qualitative zeroth-order extension to other nuclei. On the next level, the surface parameters could be determined empirically for a lighter nucleus and then the parameters could be interpolated and extrapolated to other nuclei using, for example, the relationship $X_{p/n}(N, Z)=X_0 \pm X_1(N-Z)/A + X_2 A^{1/3}$ where X stands for the well depth, radius and diffuseness parameters. This method has been used for the Woods–Saxon potential by Streets *et al* (1982). However, ultimately the surface potential should depend self-consistently on the densities. This might be achieved by a modification of the Skyrme HF potential, perhaps by letting the Skyrme parameters themselves depend on the radius.

Further tests of the models and ideas presented here may be provided by the density and moment variations of the charge distribution upon the addition or subtraction of valence nucleons around ^{208}Pb. A recent analysis of the charge density change between ^{206}Pb and ^{205}Tl observed in electron scattering (Cavedon *et al* 1982) has been used to show the validity of the Hartree–Fock independent-particle model even at large density in the nuclear interior. Other recent experiments show the more subtle effects of the addition of valence neutrons on the change in the charge distribution (Martorell and Sprung 1980, Thompson *et al* 1982).

References

Bauer M, Hernandez-Saldana E, Hodgson P E and Quintanilla J 1982 *J. Phys. G: Nucl. Phys.* **8** 525

Bear K and Hodgson P E 1978 *J. Phys. G: Nucl. Phys.* **4** L287

Beiner M, Flocard H, Van Giai N and Quentin P 1975 *Nucl. Phys.* A **238** 29

Bernard V and Mahaux C 1981 *Phys. Rev.* C **23** 888

Bernard V and Van Giai N 1979 *Nucl. Phys.* A **327** 397

—— 1980 *Nucl. Phys.* A **348** 75

Bertsch G F and Kuo T T S 1968 *Nucl. Phys.* A **112** 204

Brown B A, Massen S E and Hodgson P E 1979 *J. Phys. G: Nucl. Phys.* **5** 1655

Brown G E, Dehesa J S and Speth J 1979 *Nucl. Phys.* A **330** 290

Brown G E, Gunn J H and Gould P 1963 *Nucl. Phys.* **46** 598

Cavedon J M, Frois B, Goutte D, Huet M, Leconte Ph, Papanicolas C N, Phan X-H, Platchkov S K, Williamson S, Boeglin W and Sick I 1982 *Phys. Rev. Lett.* **49** 978

Chandra H and Sauer G 1976 *Phys. Rev.* C **13** 245

Chapman R 1982 Private communication

Chu-Hsia L and Klemt V 1981 *Nucl. Phys.* A **364** 93

Dechargé J 1981 Distributions de densités de nucleons calculées par la méthode Hartree–Fock–Bogolyubov pour les noyaux sphériques (*Centre d'Etudes de Bruyères-le-Châtel Preprint*)

Dechargé J, Girod M, Gogny D and Grammaticos B 1981 *Nucl. Phys.* A **358** 203c

Dechargé J and Gogny D 1980 *Phys. Rev.* C **21** 1568

Dover C B and Van Giai N 1972 *Nucl. Phys.* A **190** 373
Euteneuer H, Friedrich J and Voegler N 1976 *Phys. Rev. Lett.* **36** 129
Franey M A, Lilley J S and Phillips W R 1979a *Nucl. Phys.* A **324** 193
—— 1979b Private communication
Friar J L and Negele J W 1973 *Nucl. Phys.* A **212** 93
—— 1975 *Adv. Nucl. Phys.* **8** 219
Friedrich J 1980 Private communication
Frois B, Bellicard J B, Cavedon J M, Huet M, Leconte P, Ludeau P, Nakada A, Ho P Z and Sick I 1977 *Phys. Rev. Lett.* **38** 152
Gales S, Crawley G M, Weber D and Zwieglinski 1978 *Phys. Rev.* C **18** 2475
Guillot J, Van de Wiele J, Langevin-Joliot H, Gerlic E, Didelez J P, Duhamel G, Perrin G, Buenerd M and Chauvin J 1980 *Phys. Rev.* C **21** 879
Heisenberg J, Hofstadter R, McCarthy J S, Sick I, Clark B C, Herman R and Ravenhall D G 1969 *Phys. Rev. Lett.* **23** 1402
Hodgson P E 1979 *Atomki Közlemények* **21** 165
Hoffmann G W, Ray L, Barlett M, McGill J, Adams G S, Igo G J, Irom F, Wang A T M, Whitten C A, Boudrie R L, Amann J F, Glashausser C, Hintz N M, Kyle G S and Blanpied G S 1980 *Phys. Rev.* C **21** 1488
Hoffmann G W, Ray L, Barlett M L, Fergerson R, McGill J, Milner E C, Seth K K, Barlow D, Bosko M, Iverson S, Kaletka M, Saha A and Smith D 1981 *Phys. Rev. Lett.* **47** 1436
Jenkins D, Powers R J, Martin P, Miller G H and Welsh R E 1971 *Nucl. Phys.* A **175** 73
Kessler D, Mes H, Thompson A C, Anderson H L, Dixit M S, Hargrove C L and McKee R J 1975 *Phys. Rev.* C **11** 1719
Körner H J and Schiffer J P 1971 *Phys. Rev. Lett.* **27** 1457
Lanford W A and Crawley G M 1974 *Phys. Rev.* C **9** 646
Lejeune A 1980 *Nucl. Phys.* A **339** 317
Martin M J 1977 *Nuclear Data Sheets* **22** 545
Martorell J and Sprung D W L 1980 *Z. Phys.* A **298** 153
Negele J W 1970 *Phys. Rev.* C **1** 1260
—— 1974 *Phys. Rev.* C **9** 1054
Negele J W and Riska D O 1978 *Phys. Rev. Lett.* **40** 1005
Negele J W and Vautherin D 1972 *Phys. Rev.* C **5** 1472
Negele J W, Zamick L and Varma G K 1979 *Comments in Nuclear and Particle Physics* **8** 135
Perey G and Buck B 1962 *Nucl. Phys.* **32** 353
Sartor R and Mahaux C 1980 *Phys. Rev.* C **21** 2613
Satchler G R 1971 *Phys. Rev.* C **4** 1485
Schiffer J P and Körner H J 1973 *Phys. Rev.* C **8** 841
Schmorak M R 1977 *Nuclear Data Sheets* **22** 487
Sick I 1974 *Nucl. Phys.* A **218** 509
—— 1980 Private communication
Smith S M, Roos P G, Moazed C and Berstein A M 1971 *Nucl. Phys.* A **173** 32
Sprung D W L, Martorell J and Campi X 1976 *Nucl. Phys.* A **268** 301
Streets J, Brown B A and Hodgson P E 1982 *J. Phys. G: Nucl. Phys.* **8** 839
Thompson R C, Anselment M, Bekk K, Göring S, Hanser A, Meisel G, Rebel H, Schatz G and Brown B A 1982 High resolution measurements of isotope shifts and hyperfine structure in stable and radioactive lead isotopes (*Karlsruhe Preprint*)
Van Niftrik G 1969 *Nucl. Phys.* A **131** 574
Vautherin D and Brink D M 1972 *Phys. Rev.* C **5** 626
Wapstra A H and Bos K 1977 *Atomic and Nuclear Data Tables* **19** 177
Warwick A, Chapman R, Durell J L, Mo J N, Kuehner J A and Skensved P 1981 *Nucl. Phys.* A **356** 33
Whitten C A, Stein N, Hollard G E and Bromley D A 1969 *Phys. Rev.* **188** 1941
Woods P W, Chapman R, Mo J N, Skensved P and Kuehner J A 1982a *Phys. Lett.* **116B** 320
—— 1982b Private communication